Calibration of an SKA-Low Prototype Station Using Holographic Techniques

Jishnu N. Thekkeppattu[1] [ID], **Randall B. Wayth[1]** [ID], **and Marcin Sokołowski[1]** [ID]

[1]International Centre for Radio Astronomy Research (ICRAR), Curtin University, Bentley, WA, Australia

Abstract Performance of digitally beamformed phased arrays relies on accurate calibration of the array by obtaining gains of each antenna in the array. The stations of the Square Kilometer Array-Low (SKA-Low) are such digital arrays, where the station calibration is currently performed using conventional interferometric techniques. An alternative calibration technique similar to holography of dish based telescopes has been suggested in the past. In this paper, we develop a novel mathematical framework for holography employing tensors, which are multi-way data structures. Self-holography using a reference beam formed with the station under test itself and cross-holography using a different station to obtain the reference beam are unified under the same formalism. Besides, the relation between the two apparently distinct holographic approaches in the literature for phased arrays is shown, and we show that under certain conditions the two methods yield the same results. We test the various holographic techniques on an SKA-Low prototype station Aperture Array Verification System 2 (AAVS2) with the Sun as the calibrator. We perform self-holography of AAVS2 and cross-holography with simultaneous observations carried out with another station Engineering Development Array 2. We find the results from the holographic techniques to be consistent among themselves as well as with a more conventional calibration technique.

1. Introduction

The Square Kilometer Array (SKA) is an upcoming radio telescope, with its low frequency section (SKA-Low) being built in the Inyarrimanha Ilgari Bundara (Murchison Radio-astronomy Observatory) in Western Australia. The telescope will consist of 512 phased arrays called stations, with each station having 256 closed spaced dual-polarization log-periodic antennas (Bolli et al., 2020). The individual antenna voltages are digitized and added in the back-end firmware with appropriate beamweights to steer, and potentially shape, the beam in real-time. For accurate beamforming, the complex receive path gain of each antenna in a station must be accurately known. Obtaining the gain of each antenna in a station and its associated signal chain, called station calibration, is currently carried out on SKA-Low prototype stations Aperture Array Verification System 2 (AAVS2, van Es et al., 2020) and Engineering Development Array 2 (EDA2, Wayth et al., 2022) with mid-day observations of the Sun collecting intra-station visibilities. This is followed by conventional gain calibration techniques such as `mfcal` task implemented in the `miriad` radio astronomy package (Sault et al., 1995) to derive the gains (Benthem et al., 2021; Macario et al., 2022; Sokolowski et al., 2021; Wayth et al., 2022).

However, station calibration using visibilities makes use of only the intra-station baselines from a station of ~35 m diameter. Even with a multi-station telescope, the interferometric station calibration would still be unable to take advantage of the other stations, as visibilities between individual antennas belonging to different stations are difficult to compute and store. As an alternative to conventional interferometric calibration of phased arrays, holographic techniques have been suggested. Variants of holographic techniques have been successfully applied to calibrate a variety of phased array telescopes such as LOFAR (Salas et al., 2020) and EDA2 (Kiefner et al., 2021). Holography has also been proposed as a potential calibration method for the mid-frequency aperture arrays (MFAA) for the second phase of the SKA (Wilke et al., 2022). An attractive feature of holography is that it does not require the array covariance matrix, which can be beneficial for large arrays such as the MFAA (Wilke et al., 2022), although in this paper we show that holography can be carried out with such a covariance matrix, if available. Conventional holography of dish antennas uses two distinct antennas with one acting as a reference (Scott & Ryle, 1977). However, in the context of all-digital phased arrays, holographic techniques have been developed predominantly for self-holography in which the reference beam is provided by the same phased array.

Table 1
List of Holographic Techniques

Holographic technique	Reference beam source	Output
Self-holography with Beam-Correlation	Self-generated	Aperture image (2D)
Self-holography with Antenna-Correlation	Self-generated	Measured correlations (1D)
Cross-holography with Beam-Correlation	Different antenna	Aperture image (2D)
Cross-holography with Antenna-Correlation	Different antenna	Measured correlations (1D)

There are two distinct self-holographic techniques for phased arrays in the literature. The first technique, described in Wijnholds (2017), correlates each individual antenna with the reference beam. As shown in the same work, these "measured correlations" are then proportional to the receive path gains and can be solved for, if signal to noise ratio is high. Wilke et al. (2021) discusses the calibratability of phased arrays via this approach, where the effects of interfering sources are also discussed. They also apply self-holography to multiple telescopes. We will henceforth refer to this technique as the "Antenna-Correlation" approach in this paper, as the individual antennas are correlated with the reference beam. The second technique for self-holography, described in Kiefner et al. (2021), forms a reference beam and correlates it with voltage beams over a raster scan pattern on the sky. This method is closer to the more conventional holographic technique typically applied to dish antennas. The correlation of the beams over the sky results in "Beam-Correlation," a matrix that is subsequently Fourier transformed to obtain the complex aperture image. The output of this technique is an image with the antenna positions weighted by their relative complex gains, from which the individual receive path gains can be extracted. We will henceforth refer to this technique as the "Beam-Correlation" approach in this paper. Regardless of the chosen approach, implementation of self-holography for phased arrays hitherto required collection of individual antenna voltages.

For both Antenna-Correlation and Beam-Correlation techniques, replacing the self-generated reference beam with a beam obtained from a physically separate antenna system leads to cross-holography. Thus, four different phased array holographic techniques are possible, which are listed in Table 1.

In this paper, we further develop the technique used in Kiefner et al. (2021) to include self and cross-holography. We bring self and cross holographic techniques under the same framework and discuss their relative merits and demerits. We show that self-holography using Beam-Correlation can be performed with the visibilities alone. It is also shown that the two apparently distinct holographic approaches described in Wijnholds (2017) and Kiefner et al. (2021) are equivalent in their outcomes. As a demonstration of the techniques, we perform holography of the AAVS2. Both self and cross holographies are performed, and the results compared with `mfcal`. As this paper focuses on applying holography to calibrate the digitally beamformed SKA-Low stations, we will use the terms station, phased array or antenna array interchangeably to refer to these phased arrays.

2. Tensors for Signal Processing

The theoretical framework developed in this paper makes use of multi-way data structures, also known as *tensors* in the signal processing literature. While the expressions for holography can be written out without resorting to tensors, the use of tensors makes the equations tractable and provides novel insights into the technique.

The following definitions are used in this paper. We would like point out that there are multiple (and often inconsistent) definitions of tensors and associated data structures in the literature.

1. Arrays with any number of indices are referred to as tensors and denoted by calligraphic uppercase letters, such as $\mathcal{W}$. The total number of indices required to specify an element of a tensor is called its *order* (Kolda & Bader, 2009). Confusingly, the order of a tensor is also referred as its *rank* sometimes, though the rank of a tensor can also denote a concept similar to matrix rank.
2. The elements constituting a tensor are denoted by the same letter as the tensor, but in plain lowercase with Greek alphabet indices, such as $w_{\alpha\beta}$. These indices can appear as subscript ($v_{\eta\tau}$), superscript ($v^{\eta\tau}$) or both $\left(v_\tau^\eta\right)$. In this aspect, we deviate from the convention prevalent in signal processing where only subscripts are used (e.g., Costa & Haykin, 2010), and adopt the tensor convention more common in physical sciences (e.g., Misner et al., 1973)

3. Vectors are denoted by bold lowercase letters, such as $\boldsymbol{x}$. An element of a vector is denoted by a plain lowercase letter with a Greek alphabet index variable, such as x_η.
4. Matrices are denoted by boldfaced uppercase letters such, as $\boldsymbol{W}$. Tensors of second-order can be represented by matrices.

2.1. Einstein Summation

We make use of Einstein summation for tensor operations. When Einstein summation is employed, identical indices appearing in *both subscript and superscript* of the terms are summed over. Consequently, the index that is summed over is a *dummy index* and may be replaced with a different letter. The indices of a tensor may need to be *raised* or *lowered* for summation, which is achieved by contracting with the *metric* tensor. The metric for the tensors used in this paper is Euclidean, with $\delta_{\eta\gamma}$ defining the metric. In other words, the metric can be represented by an identity matrix and therefore, raising or lowering of the indices is a trivial exercise.

3. Tensor Formulation of Phased Array Holography

In this section we formulate holography using tensors which is applicable to both self and cross holographic techniques. We demonstrate that the distinct approaches to self-holography—namely the Beam-Correlation method and Antenna-Correlation method—yield the same results, although the former provides a 2D aperture image. We also show that self-holography can be carried out with visibilities alone.

We begin with formulating the Beam-Correlation holography method. In order to perform holography with phased arrays, the voltage beam of the station to be calibrated is scanned in a raster, and correlated with a reference beam pointed toward a strong source to obtain a sky image called the Beam-Correlation around the source. Scanning requires pointing the voltage beam of the station toward each grid point on a pattern on the sky by a weighted addition of the individual antenna voltages. The phased array consists of N individual antennas, each with an associated complex receive path gain g_η; $\eta \in [0, N-1]$. From each antenna numbered η, a stream of voltages v_τ^η is acquired, with τ being the time index and T being the total number of samples collected. Using Einstein summation, the collected voltages can be written as

$$v_\tau^\eta = \delta_{\chi\phi}^\eta g^\phi s_\tau^\chi; \tau \in [0, T-1] \tag{1}$$

$$\delta_{\chi\phi}^\eta = \begin{cases} 1, \eta = \chi = \phi \\ 0, \text{otherwise} \end{cases} \tag{2}$$

where the third-order tensor $\delta_{\chi\phi}^\eta$ defined by Equation 2 assists in performing Hadamard like multiplications, with χ and ϕ as dummy indices. It may also be noted that in Equation 1, we changed the dummy index of g_η to ϕ and subsequently raised that index. s_τ^χ denote the voltages that would be collected if the system was ideal such that no gain calibration is required. It also includes the noise added by the receiver chain, especially the noise contributions from the low noise amplifiers referenced to the system input. The receiver noise can also be explicitly included, however as we show in Section 4.1, it manifests in autocorrelations alone and can safely be ignored, especially for cross-holography. Equation 1 can also be written in linear algebra notation as $\boldsymbol{v}_\eta = g_\eta \boldsymbol{s}_\eta$ for each antenna, where g_η is the gain of antenna η.

The complex weights required to beamform the station to a grid of direction cosines l, m on the sky can be organized into a third-order tensor $\mathcal{W}$ with elements $w_{\alpha\beta\eta}$. We assume the station to be a planar array. Then, for a direction cosine pair l_α, m_β in the sky, the corresponding weight $w_{\alpha\beta\eta}$ to steer the voltage beam is

$$w_{\alpha\beta\eta} = \exp\left[j2\pi\{x_\eta l_\alpha + y_\eta m_\beta\}\right], \tag{3}$$

where x_η, y_η is the location of antenna η in the aperture plane, in units of wavelengths. The third-order tensor of station voltage beams $\mathcal{D}$ over a raster pattern in the sky can then be written as,

$$d_{\alpha\beta\tau} = w_{\alpha\beta\eta}\delta_{\chi\phi}^\eta z^\phi v_\tau^\chi. \tag{4}$$

where z is the steering vector of complex weights required to point the beam toward the calibrator. The multiplication of the antenna voltages with the steering vector removes the geometric phase for an off-boresight calibrator and brings it to the phase center, ensuring that the Beam-Correlation is centered on the source.

The Beam-Correlation B is obtained by cross-correlating the reference beam voltages with the scanned beams and temporal averaging. For the cross-correlation to be meaningful, the reference beam voltages as well as the scanned beam voltages must be sampled at the same time, or interpolated to be aligned. The vector consisting of the complex voltages from the reference antenna can be written as r and thus the generation of the Beam-Correlation becomes

$$b_{\alpha\beta} = w_{\alpha\beta\eta} \delta^\eta_{\chi\phi} z^\phi v^\chi_\tau (r^*)^\tau,$$
(5)

where for brevity we have omitted a multiplicative factor of $1/T$, required for temporal averaging. This omission will result in an overall scaling factor requirement for absolute flux density calibration, however the relative gain measurements will be unaffected. We now define a vector of "measured correlations" h, such that

$$h^\eta = \delta^\eta_{\chi\phi} z^\phi v^\chi_\tau (r^*)^\tau$$
(6)

is the cross-correlation between the antenna numbered η and the reference beam. Then Equation 5 can be written compactly as

$$b_{\alpha\beta} = w_{\alpha\beta\eta} h^\eta.$$
(7)

Equation 7 describes a generalized form of holography, where the Beam-Correlation can be obtained from a vector of "measured correlations" h. It is worth noting that these measured correlations h are used in the Antenna-Correlation holographic method to obtain the gains (Wijnholds, 2017).

To obtain the complex aperture image A, a Fourier transform of the Beam-Correlation B is taken. For this, we define a fourth-order "Fourier transform tensor" $\mathcal{F}$ such that

$$f^{\alpha\beta}_{\mu\sigma} = \exp\left[-j2\pi(x_\mu l_\alpha + y_\sigma m_\beta)\right].$$
(8)

where μ and σ are the indices for the two orthogonal coordinates x and y in the aperture image plane. The aperture image can be written as

$$\begin{aligned} a_{\mu\sigma} &= f^{\alpha\beta}_{\mu\sigma} b_{\alpha\beta} \\ &= f^{\alpha\beta}_{\mu\sigma} w_{\alpha\beta\eta} h^\eta. \end{aligned}$$
(9)

In Equation 9 the Fourier transform is *independent* of the summation over the index η, and therefore can be treated separately for each antenna. In other words, each slice of the weight tensor $\mathcal{W}$ may be Fourier transformed separately. Thus, we can evaluate the Fourier transform of a slice of the weight tensor for each antenna η. In Equation 10, we combine the Fourier and beam-weight terms of Equation 9 by substituting Equations 3 and 8 and invoke the summation symbol explicitly for clarity,

$$a_{\mu\sigma} = \sum_\eta h_\eta \left(\sum_\alpha \sum_\beta \exp\left[j2\pi\{(x_\eta - x_\mu)l_\alpha + (y_\eta - y_\sigma)m_\beta\}\right] \right).$$
(10)

It is easy to observe that the operation in Equation 10 is similar to a Fourier transform of sinusoids, resulting in delta functions in the Fourier plane. It can be seen that for a given η, when μ and σ are such that $x_\mu = x_\eta$ and $y_\sigma = y_\eta$ corresponding to the location of the antenna η in the aperture image, the exponential term becomes unity. As long as the direction cosines l and m span a large range, the double summation over the exponential approaches zero when $x_\mu \neq x_\eta$ and $y_\sigma \neq y_\eta$. Thus, we may write

$$a(x_\mu = x_\eta; y_\sigma = y_\eta) \propto h^\eta.$$
(11)

Substituting Equation 1 in Equations 6 and 11 becomes

$$a(x_\mu = x_\eta; y_\sigma = y_\eta) \propto \delta^\eta_{\chi\phi} z^\phi \delta^\chi_{\zeta\psi} g^\psi s^\zeta_\tau (r^*)^\tau.$$
(12)

Equation 12 can then be rewritten in linear algebra as follows to enable an easier interpretation;

$$a(x_\mu = x_\eta; y_\sigma = y_\eta) \propto z_\eta g_\eta \boldsymbol{s_\eta} \boldsymbol{r}^*, \tag{13}$$

where $z_\eta g_\eta \boldsymbol{s_\eta}$ is the $1 \times T$ row vector of complex voltages from antenna η, including the corresponding complex gain g_η and steering coefficient z_η, $\boldsymbol{r}$ is the $T \times 1$ column vector of complex reference beam voltages. Thus the interpretation of Equations 12 and 13 is that the aperture image obtained from holography consists of scaled versions of the complex correlation between the reference beam and individual antennas at the corresponding antenna locations.

We may now extract the relative receive path gains k^η from the aperture image as

$$k^\eta = a(x_\mu = x_\eta; y_\sigma = y_\eta) \propto h^\eta. \tag{14}$$

As the reference beam is common for all the antennas, the complex measured correlations at the antenna locations differ only by their relative receive path gains and variations in their embedded element patterns (EEPs) toward the calibrator. If the EEPs are all identical, the gains obtained from holography will be proportional to the receive path such that $k^\eta \propto g^\eta$. Also, the relation between the aperture image $a_{\mu\sigma}$ at the antenna locations and the measured correlations h^η show that the gains obtained from Beam-Correlation holography ought to be similar to those from the Antenna-Correlation method, except for multiplicative constants. Thus, the key takeaway messages from our analysis are as follows.

1. The Beam-Correlation in Equation 7 is an inverse Fourier transform of the antenna locations weighted by the corresponding measured correlation.
2. Consequently, a Fourier transform of the Beam-Correlation results in the measured correlations from the Antenna-Correlation method.

In writing Equations 10–14, an assumption is made that there are pixels in the aperture image corresponding to the exact antenna locations. In practice, the resolution of the aperture image is limited by the extent of l, m scan. If the pixels do not correspond precisely to the antenna locations, scalloping will be seen in the aperture image. The effects of such leakage can be reduced with a combination of windowing and padding the Beam-Correlation to hyper-resolve the aperture image as done in Section 6.1. As shown in the same section, the gains can be obtained from such an aperture image by taking an average of the pixels around an antenna locations, with the number of pixels to be averaged determined by the windowing used.

Thus, either the measured correlations or the values from the antenna locations in the aperture image are useful for calibration, except for an overall scaling factor required to fix the flux density scale. A similar conclusion was reached in Wijnholds (2021), albeit with a different modeling. The use of these gains is application dependent. For all-sky imaging with individual SKA-low stations, the gains can be used to calibrate the visibilities, for example, by supplying them as `gains` file in a `miriad` data set. On the other hand if the stations are used in beamformed mode, which is the expected use case for the SKA-low stations, the gains have to be used when the weights are calculated when the voltage beam is formed.

4. Self-Holography

The reference beam in self-holography can be written as

$$r^\tau = z_\gamma v^{\gamma\tau} \tag{15}$$

where $\boldsymbol{z}$ is the vector of complex weights required to phase the beam toward the calibrator. This results in

$$
\begin{aligned}
b_{\alpha\beta} &= w_{\alpha\beta\eta} \delta^\eta_{\chi\phi} z^\phi v^\chi_\tau z^*_\gamma (v^*)^{\gamma\tau} \\
&= w_{\alpha\beta\eta} \delta^\eta_{\chi\phi} z^\phi v^\chi_\tau (v^*)^{\gamma\tau} z^*_\gamma \\
&= w_{\alpha\beta\eta} \delta^\eta_{\chi\phi} z^\phi c^{\chi\gamma} z^*_\gamma
\end{aligned} \tag{16}
$$

where we rearrange terms and identify $c^{\chi\gamma} = v^\chi_\tau (v^*)^{\gamma\tau}$ as the time averaged cross-correlation—visibility—between antennas χ and γ. The second-order tensor of visibilities can be represented as a correlation matrix $\boldsymbol{C}$. Comparing Equation 16 with Equation 7, it can be observed that the measured correlations $\boldsymbol{h}$ can be obtained in self-holography from the correlation matrix,

$$h^\eta = \delta^\eta_{\chi\phi} z^\phi c^{\chi\gamma} z^*_\gamma. \tag{17}$$

Equations 16 and 17 show that the formation of the measured correlations, and consequently Beam-Correlation and aperture imaging, are all possible using visibilities alone for self-holography. While visibilities are computationally expensive compared to holography, the fact that they are useful for self-holography implies that direct comparisons can be made between various holography algorithms and conventional calibration techniques.

4.1. Effect of Autocorrelations

The correlation matrix in self-holography is Hermitian, with receiver noise power dominated autocorrelations occupying the diagonal. If all the antennas have similar receiver noise, the autocorrelations will be similar across the antennas. However, for closely spaced antennas some amount of receiver noise gets coupled across antennas and can appear as an additional noise power in the cross-correlations, which is also a function of the antenna separation. Moreover the autocorrelations also contain the average component of the radio sky, particularly the diffuse emission from the Galaxy which is a function of the local sidereal time. It is therefore imperative that the effect of autocorrelations on the calibration results is understood.

For this, we assume that the correlation matrix is diagonal, consisting of receiver noise powers alone as autocorrelations and no signal originating in the sky. We write this as $c^{\chi\gamma} = 0, \forall \chi \neq \gamma$. We further assume that the steering is toward the boresight of the station, which implies $z^*_\gamma = 1$. This gives the measured correlations as $h = \mathrm{diag}(C)$. However, as already noted in Equation 14, $k^\eta \propto h^\eta$. Therefore in the general case, the gain obtained for each antenna will be biased by the excess power in its autocorrelations, as self-holography is essentially a linear operation on the correlation matrix as shown in Equation 17. This bias could be substantial if the calibrator does not have sufficiently high flux densities so as to overcome the combined effects of the diffuse sky and the receiver noise. A potential solution to mitigate this bias is to split a station into two logical sub-arrays, form a reference beam with one of the sub-arrays and use it to calibrate the other sub-array. Yet another potential solution within the paradigm of self-holography is an application of subspace filtering to extract data pertaining to the calibrator alone from the correlation matrix. However instead of these techniques, we propose cross-holography using a second phased array to provide the reference beam. This is discussed in Section 5.

Nonetheless, for an N antenna array the contribution of the autocorrelation terms to the gains is diminished by a factor of N upon summation as per Equation 17. Therefore, if a calibrator with high flux density such as the Sun is employed, autocorrelations will not be substantially higher than cross-correlations and the bias can be expected to be minimal. This was pointed out, in a qualitative sense, in Kiefner et al. (2021).

5. Cross-Holography

An alternative to self-holography is using a reference beam from a nearby reference antenna, which is also far enough from the station under test to avoid cross-talk. With cross-holography, the short intra-station baselines and autocorrelations do not contribute to the calibration. Using mathematics similar to the one in Section 4 this can be shown by elementary means if another phased array provides the reference beam. Therefore, while self-holography can potentially be biased by the excess power appearing in the autocorrelations and short intra-station baselines, cross-holography would be immune to receiver noise powers, and relatively insensitive to large-scale diffuse structures which resolve out on the longer inter-station baselines.

Similar to self-holography, cross-holography can be carried out with either Beam-Correlation or Antenna-Correlation. However, the inter-station visibilities between the antennas belonging to different stations are not available in general and therefore the correlation matrix approach is seldom a viable option for Beam-Correlation holography.

6. Holography Applied to AAVS2

In this section, we perform self and cross-holography of AAVS2. For cross-holography the reference beam is provided by the EDA2 station. The data were acquired on 30 November 2022, from 04:47 UTC onward. The Sun was chosen as the calibrator, and the observation frequency was centered on 159.375 MHz. Data were collected from a single polyphase filterbank (PFB) coarse channel of ~925 kHz bandwidth (Comoretto et al., 2017).

The observations were carried out with the stations operating in different modes. AAVS2—the station to be calibrated—was configured to perform voltage dumps of 262,144 complex samples, corresponding to about 0.28 s, from all the antennas every few seconds. For this work, we use one voltage dump data set. EDA2, the station providing the reference beam, was configured to collect the complex station beam voltage data in `psrdada` format (van Straten et al., 2021), with the beam pointing toward the Sun. As the two systems share a common clock source and have identical channelizing schemes, the data from AAVS2 and EDA2 are coherent and suitable for cross-holography. Additionally a `csv` file consisting of the locations of the antennas within AAVS2, obtained during the station deployment, is used to perform station voltage beam scan required for Beam-Correlation. The various holographic techniques are implemented in `python`. The tensor operations are carried out with the use of `numpy` package, specifically **numpy.einsum** is used for various operations involving large tensors. We first perform self-holography with the AAVS2 data alone, followed by cross-holography including the EDA2 data.

### 6.1. Self-Holography of Aperture Array Verification System 2

In order to validate the mathematics developed in Sections 3 and 4, we perform self-holography with AAVS2 using the following three methods.

1. Beam-Correlation from voltage dumps: We perform self-holography with voltage dumps using the same procedure outlined in Kiefner et al. (2021) which is summarized here for completeness. The reference beam is formed from the voltages using the calculated position of the Sun over the observatory. The sky is gridded with dimensions 85×85, and the Beam-Correlation is calculated for this grid. A 2D Gaussian window of $\sigma = 1.0$ in direction cosine units giving a full width at half maximum of 2.355, is applied to the Beam-Correlation to reduce ringing artifacts in the aperture image. The Beam-Correlation is also zero padded to increase the final aperture image dimension to 513×513. Subsequently, the Beam-Correlation is Fourier transformed to obtain the complex aperture image. From the aperture image, 10 pixels surrounding each antenna location are averaged to obtain the corresponding complex gains.
2. Beam-Correlation from visibilities: The voltage data for each antenna pair are correlated to obtain the correlation matrix consisting of visibilities. The Beam-Correlation is then obtained from this matrix, using Equation 16, Fourier transformed and gains extracted as in the previous case.
3. Cross-correlating the reference beam with individual antennas: From the voltage dumps, the measured correlations are calculated as per Equation 6, where each antenna is individually correlated with the reference beam. As the measured correlations are proportional to the receive path gains, they are normalized to be used as gains for calibration.

Figure 1 shows the results from self-holography using the above three methods, along with gains obtained from `mfcal` routine in `miriad`. The various self-holographic techniques yield the same results, validating the equivalence between them. The `mfcal` routine gives gains that are broadly consistent with the various self-holography methods, further increasing our confidence in the self-holography based calibration. Pearson correlation coefficients calculated between various self-holographic techniques, as well as with cross-holography and `mfcal` are discussed in the Section 6.2.

### 6.2. Cross-Holography of Aperture Array Verification System 2 With EDA2

As AAVS2 and EDA2 are separated by ~200 m, a relative time delay is expected for a source that is away from the boresight (zenith). Besides, the different lengths of the fibers carrying the RF data to the central facility can give rise to an additional delay. Prior to performing holography, this relative delay between the data from AAVS2 and EDA2 is estimated and corrected for. In order to coarse align the two different data sets, a finite number of samples are discarded from the EDA2 data using the difference between the timestamps in the corresponding observation metadata. The voltage data from AAVS2 are then beamformed toward the Sun, the resulting voltage beam channelized with FFT and cross-correlated with the similarly channelized EDA2 voltage stream. The number of FFT channels is a trade-off between sensitivity and bandwidth de-correlation effects. We deem 64 frequency channels across the ~1 MHz bandwidth sufficient to reveal the relative delay without losing sensitivity. The phase of the resulting cross-spectrum clearly shows a linear ramp as a function of frequency, indicating a finite time delay between the stations. If the unwrapped phase gradient is more than 2π across the band, the data have to be aligned further. However, the timestamps in AAVS2 and EDA2 data are accurate enough that this is
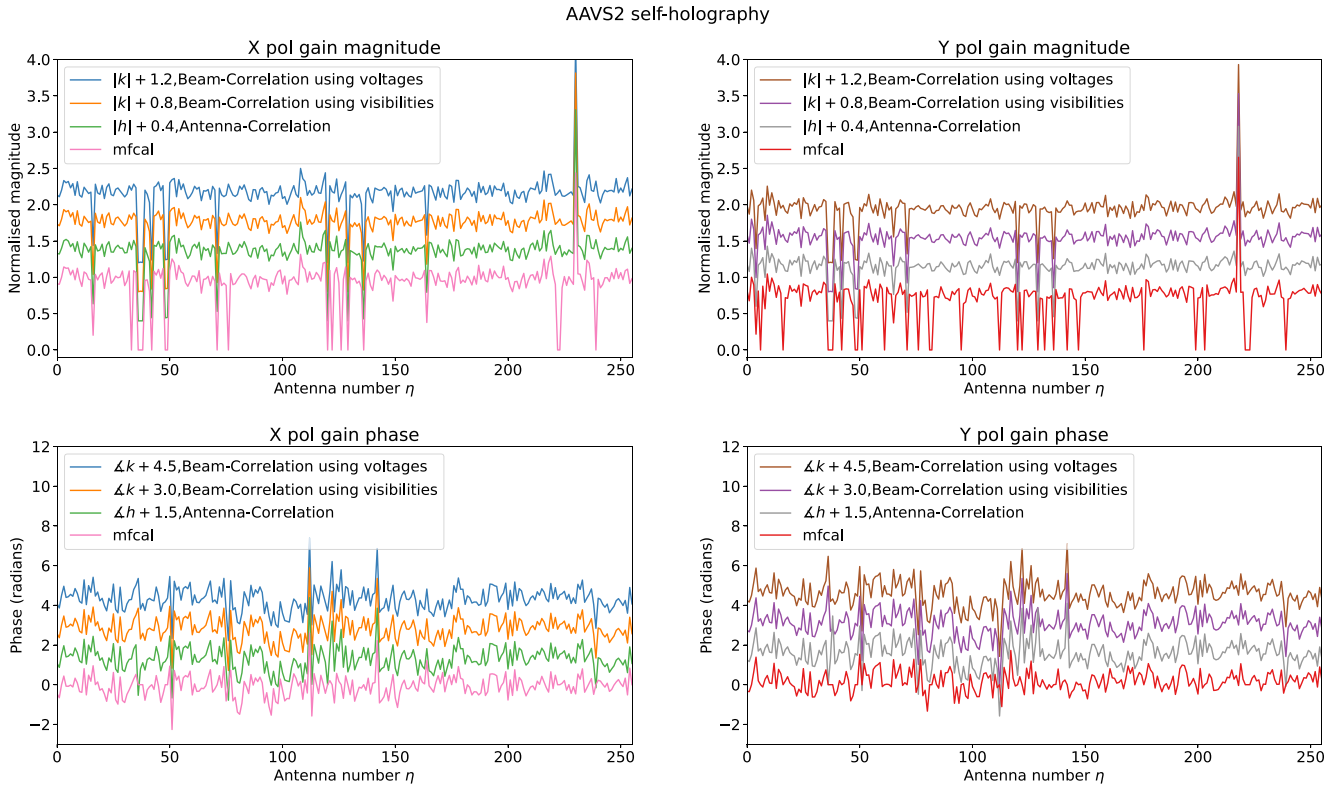
Figure 1. Complex gains obtained from multiple self-holographic techniques. Also shown are the gains as obtained from `mfcal` routine in `miriad`, for comparison. The holographic gains are normalized with antenna #3 as the reference, similar to `mfcal`. The input visibility data to `mfcal` have several outlier antennas flagged. Therefore the corresponding `mfcal` gains are set to zero as seen in the plots; however these flags are not applicable for holography. In all plots the lines are artificially offset for clarity and the offset values are indicated in the legend. The gains from self-holographic techniques show extremely good agreement with each other as well as with the `mfcal` derived gains.

not required. A straight line model is fit to this phase ramp excluding the PFB edge channels, and used to re-phase the EDA2 data to obtain the reference beam. The phases and polynomial fits to them before and after the delay correction are shown in Figure 2.

Subsequently, we perform cross-holography with both Beam-Correlation and Antenna-Correlation techniques. In Figure 3, the complex aperture images obtained from Beam-Correlation method are shown for both polarizations. Figure 4 compares the measured correlations from Antenna-Correlation cross-holography with the ones
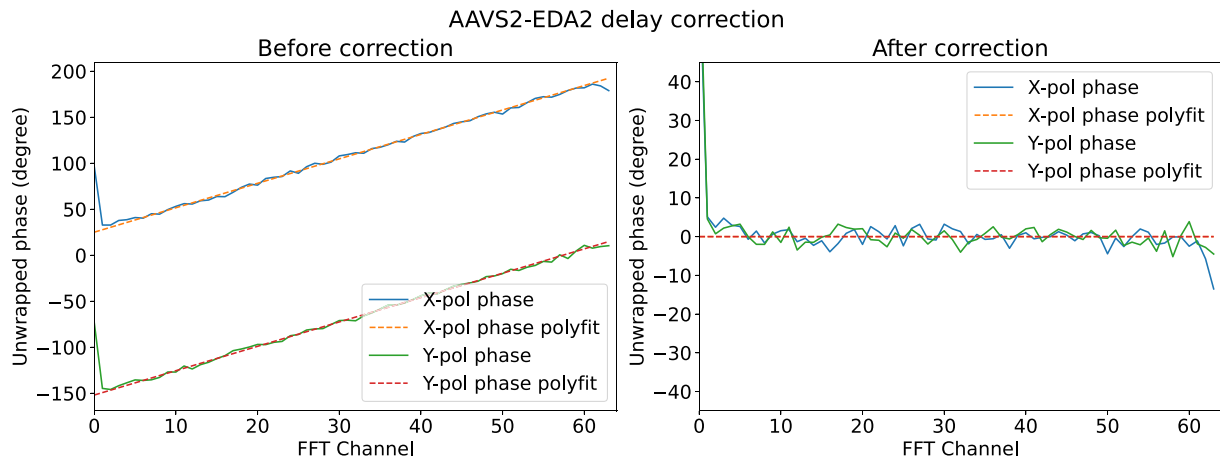
Figure 2. Inter-station delay correction for cross-holography. The plots show the AAVS2-EDA2 cross-spectrum phase. The phase can be modeled by a delay and corrected for.

from Antenna-Correlation self-holography and `mfcal`. In Figure 5, we show the Pearson correlation coefficient calculated between multiple calibration techniques, which we interpret as a measure of similarity between various techniques. Alternatively, the root-mean-square deviations (rmsd) between these quantities could also be employed, as Pearson correlation coefficient shows only a linear correlation. However rmsd is also quite sensitive to outliers. The various holographic techniques show very high correlation, which can be interpreted as them being consistent. An interesting observation is that holographic gains obtained from Beam-Correlation and Antenna-Correlation are very similar. Gains from self and cross-holographies show lower correlation, especially in their phases. Although the `mfcal` gains are correlated with holographic gains, they are not exactly the same. This is expected, as `mfcal` is fundamentally a different technique with different underlying assumptions, and several antennas had to be flagged for `mfcal` to converge. This is evident in the Y-polarization `mfcal` gains in which several antennas are flagged.

7. Discussion

The results from Sections 6.1 and 6.2 demonstrate the feasibility of applying multiple holographic techniques for calibrating the SKA-Low prototype stations. The convergence of various approaches toward identical outputs demonstrate the robustness of holographic techniques. Despite Beam-Correlation and Antenna-Correlation showing identical results, the two methods are not redundant as they serve different purposes. Owing to its simplicity, Antenna-Correlation technique can be used to obtain gains that can directly be used for station calibration. Beam-Correlation, on the other hand, provides a visual representation of the station gains where any systematics issues are easier to identify. As an example, a phase gradient would appear across the aperture image when a mis-calibration of the inter-station delay or source position causes an excess delay between two stations. In a station, the 256 antennas are aggregated into groups of 16 at the SMART boxes, where the analog RF signals are also converted from electrical to optical. These optical signals are then patched to long distance fiber connection at the field node distribution hubs for transport to the control room, where they are connected to the tile processing modules (TPM, Naldi et al., 2017)with each TPM processing signals from 16 antennas (Wayth et al., 2022). Thus, owing to this grouping of antennas into "tiles" of 16 sharing some resources, an aperture image can be useful in identifying issues pertaining to specific SMART box or TPM signal paths. Besides, the effect of any interfering source can be inferred by inspecting the Beam-Correlation, prior to any calibration and imaging. The effectiveness of the reference beam to isolate the calibrator from other sources in the sky can be verified with Beam-Correlation, as secondary sources in the sky that can potentially interfere with calibration (e.g., via sidelobes) would be visible in the Beam-Correlation. This makes the Beam-Correlation method a powerful diagnostic tool.

In general, the gains obtained from holography will be frequency and direction dependent. Therefore for broadband calibration of a station, holography (or any other calibration algorithm) has to be repeated at multiple frequencies so as to obtain the instrumental bandpass. Simulated EEPs of SKA-Low antennas in a station show considerable deviations from antenna to antenna, due to strong mutual coupling effects (Bolli et al., 2022; Davidson et al., 2019). The EEPs are distinct for each antenna, as well as each antenna EEP is a function of frequency, azimuth, and elevation. While inclusion of EEPs into holography goes beyond the scope of this paper, a potential avenue to improve calibration is inclusion of simulated EEP of each antenna to reduce the direction-dependence of the gains. The tensor formalism introduced in this paper can be extended to include such multi-dimensional EEP data. If enough compact and bright sources to sufficiently sample the azimuth and elevation are identified, cross-holography utilizing a reference antenna with accurately known beam patterns can be used to even verify the antenna EEPs.

7.1. Choosing Between Self-Holography and Cross-Holography

The results from AAVS2 holography show that the derived gains are very similar for self and cross holography, implying that the impact of auto-correlations on self-holography is minimal for a bright source. Therefore, self-holography may suffice as a viable calibration technique for SKA-Low stations when Sun is available as a calibrator. Since multi-beam capabilities are built into SKA-Low station signal processing (Caiazzo, 2017; Hampson et al., 2016), for observations demanding high accuracy one of the beams can be fixed on a calibrator and cross-correlated with each antenna within the station signal processing to track temporal gain changes in
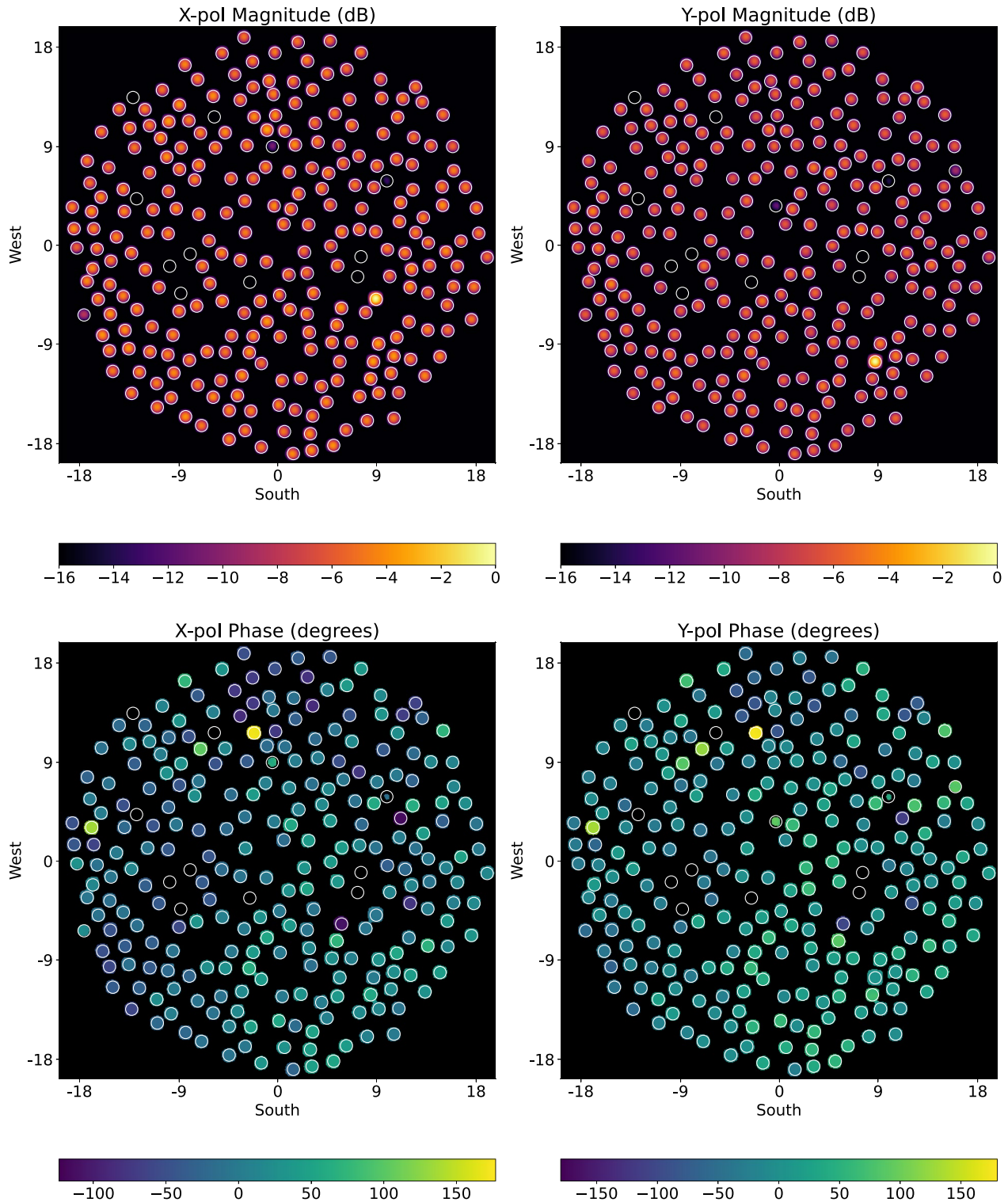
Figure 3. Aperture images from cross-holography of Aperture Array Verification System 2 with Engineering Development Array 2 reference beam. The magnitudes have been peak normalized and converted to decibels (dB) to enhance the dynamic range. All distances are in meters and the known antenna positions are circled. Also, the phase images are masked using a mask created from the magnitude images.
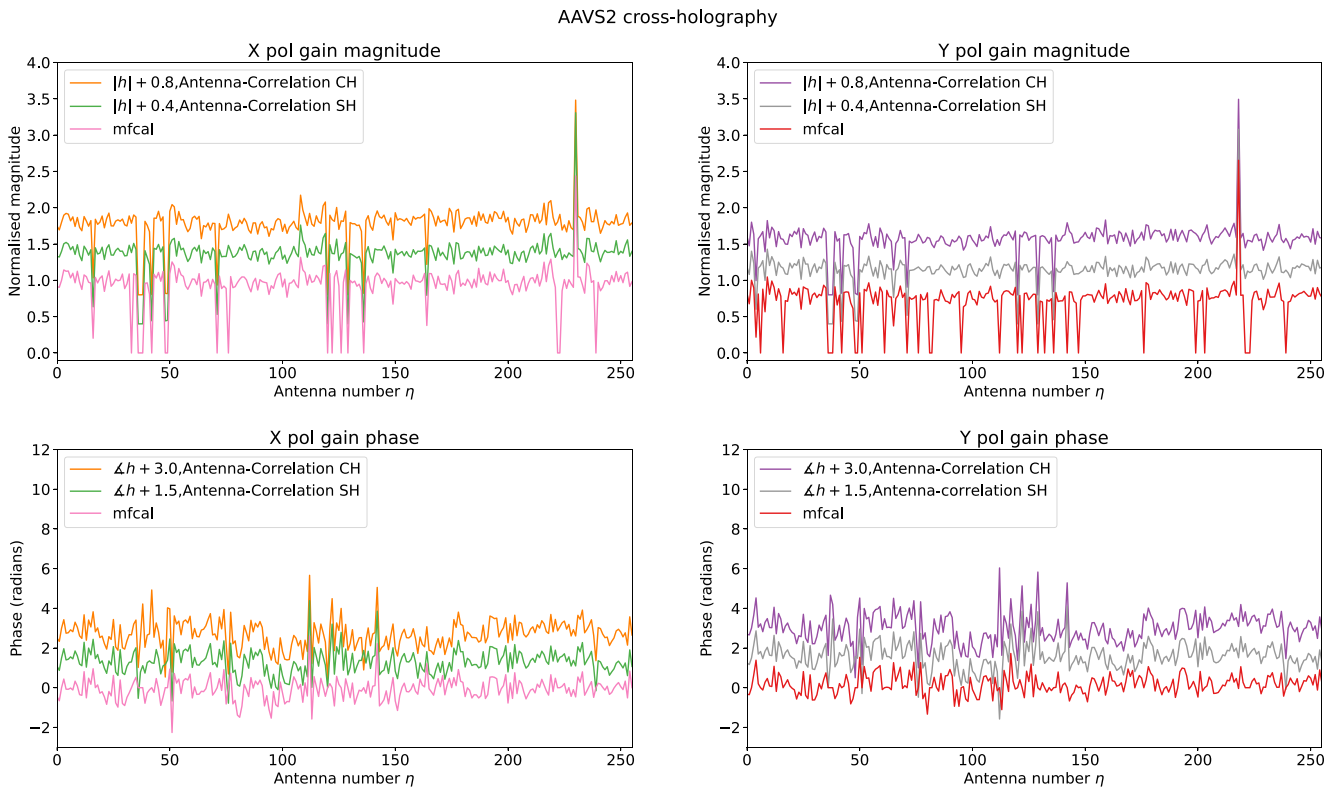
Figure 4. Comparison between the complex gains obtained from cross-holography (CH) and self-holography (SH). Shown are the measured correlations with the Antenna-Correlation approach along with the gains obtained from `mfcal` for comparison. Similar to Figure 1 the flagged `mfcal` gains are set to zero and the lines are artificially offset for clarity.

real-time. Such a near real-time station calibration is implemented in LOFAR (van Haarlem et al., 2013), however it uses the correlation matrix and not holography.

However, self-holography relies on having a reference beam that can isolate the calibrator from other sources. The SKA-Low prototype station used in this work is close to being calibrated and therefore self-holography provides excellent results. On the other hand, if a station is significantly out of calibration (especially phase/delay calibration), the Beam-Correlation would be ill-formed and self-holography would fail. In such a scenario, cross-holography with a calibrated reference station will have to be employed, such that the reference beam can isolate the calibrator.

In the early phases of SKA-Low with a limited number of baselines, an iterative approach to holographic calibration is possible. A reference beam is formed with a partially calibrated station to bootstrap the overall process and used for holography of the other stations, and finally holography of the initial station is carried out with a reference beam from one of the other stations. Alternatively, once a station is calibrated, it can be combined with previously calibrated stations to obtain a progressively narrower tied-array reference beam to calibrate rest of the stations. However, one potential issue to be considered for cross-station holography with the Sun is that at the frequencies of interest, the Sun gets resolved out on baselines longer than a few hundred meters. Therefore if cross-holography is to be used on such baselines, compact albeit weaker sources such as the A-team sources (Virgo-A, Hydra-A etc.) may be better suited. Nonetheless, cross-holography with the Sun will still be useful for a large number of SKA-Low stations which will be less than hundred meters apart, such as the closely spaced stations within the SKA-Low core or the ones within each cluster of 6 stations along the spiral arms (Dewdney & Braun, 2016).

7.2. Can Holography Provide Unknown Antenna Locations Within an Array?

A question that frequently arises in phased array holography is whether it can be used to find unknown antenna locations in an array, especially using the Beam-Correlation technique which provides an aperture image. For phased arrays, the unknowns consist of both the antenna complex gains and the antenna locations forming the
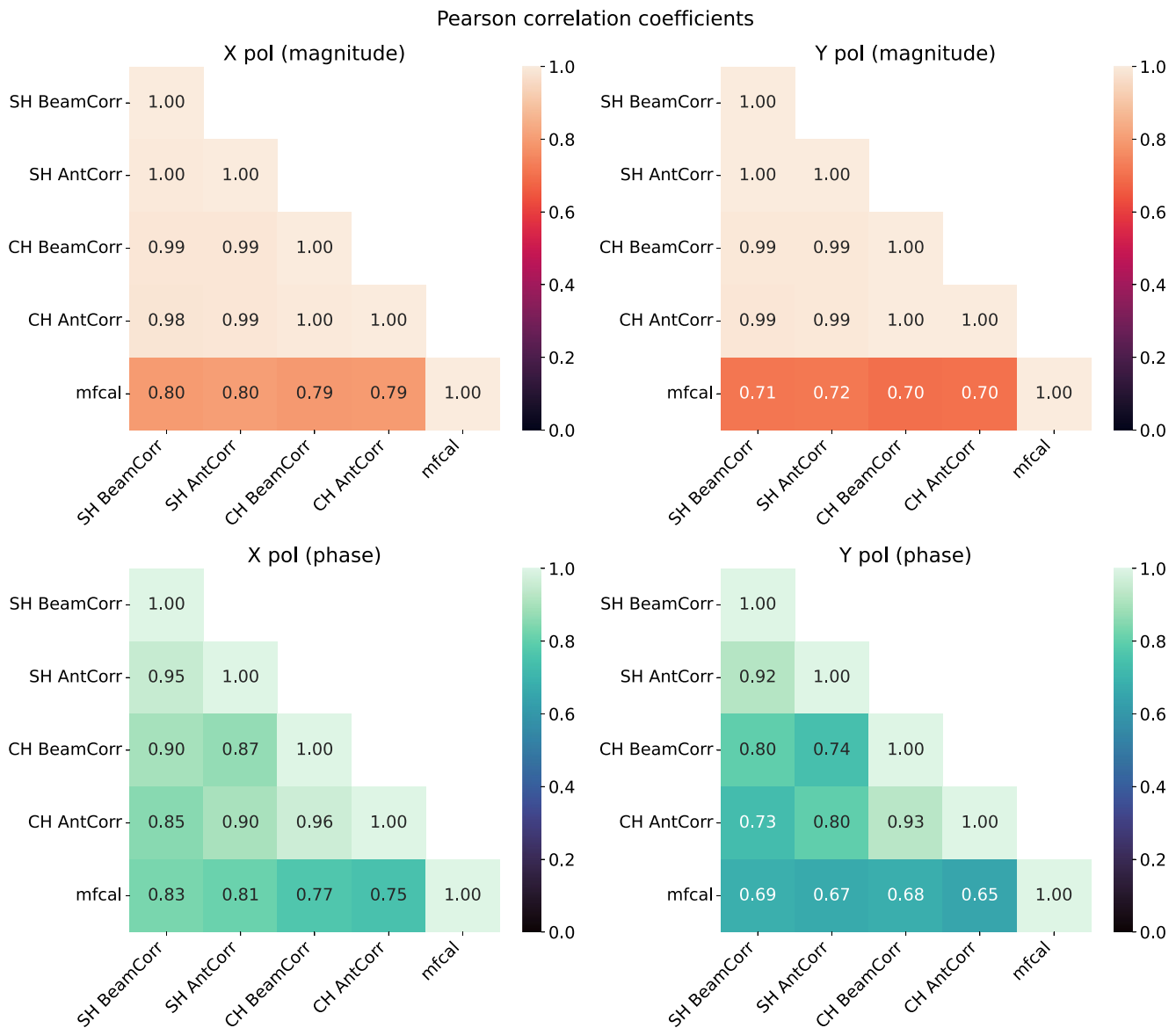
Figure 5. Pearson correlation coefficients computed between the various gains shown in Figures 1 and 4. A correlation coefficient of 1 denotes perfect correlation and 0 indicates lack of any correlation. The holographic techniques yield nearly identical gains, as shown by their high correlation. In general, the holographic gains are also consistent with mfcal gains. However they operate under different assumptions and use different algorithms, which is probably the reason for lower correlation coefficients between holographic methods and mfcal. The presence of flagged antennas in mfcal also contributes to a reduction in the correlation coefficients.

aperture. This is in contrast to dish holography where the unknown is the dish aperture alone. The dish beam scanning can be accomplished, by physically moving the aperture to be mapped. This does not require a-priori knowledge of the aperture, under the assumptions that the aperture stays the same during the antenna movements and the dish pointing model is accurate. The unknown pixels in the dish aperture image can then be solved for with sufficient number of pointings. For phased arrays, even to scan the beam to obtain the Beam-Correlation, the antenna location information is required without which the steering vectors cannot be computed.

If a sufficiently large bandwidth is used and the phase of an antenna across the band has a linear trend due to an excess delay, then it may be possible to calculate its misalignment along the baseline to the reference station. However, the positions of the antennas within the array, the cable lengths from the antennas to the digitizers, and the phases introduced by the analog electronics all contribute to the gains obtained after holography. Therefore, such a delay could also arise from excess cable lengths. Nonetheless, accurate antenna positions within each station can be obtained during deployment so that small deviations like cable delays can be absorbed into the gains.

8. Conclusions

In this work, we introduced a novel tensor based framework for phased array holography and unified multiple variants of holography, namely the Beam-Correlation and Antenna-Correlation techniques and their self and cross holography variants. The framework that we developed in this paper combined these different types of holography and shows that they are consistent among themselves and with standard interferometric calibration. The differences between self and cross holography, and the limitations related to applying self-holography to a fully uncalibrated station have also been discussed. The equations given in this paper can be extended to include multiple system non-idealities to improve calibration. The robustness of the techniques is demonstrated using on-sky data from AAVS2, and comparing the gains obtained with the ones from a more conventional interferometric calibration. The results are promising and in future, holography can potentially aid real-time station calibration of SKA-Low.

Acronyms

SKA-Low	Square Kilometer Array-Low
AAVS2	Aperture Array Verification System 2
EDA2	Engineering Development Array 2
EEP	Embedded element pattern
CH	Cross-holography
SH	Self-holography

Notation

$\mathcal{W}$	Third-order tensor of beamforming weights
$\mathcal{F}$	Fourth-order tensor for Fourier transform
$\mathcal{D}$	third-order tensor of station voltage beams over the sky
A	Complex aperture image
B	Beam-Correlation
C	Correlation matrix
x, y	Location of antennas in the aperture plane in units of wavelength
l, m	Direction cosines in the sky, with respect to the array phase center
h	Measured correlations
g	Receiver gains

Data Availability Statement

Code and data used for this paper are available in a dataset associated with this publication on Zenodo (Thekkeppattu et al., 2023).

References

Benthem, P., Wayth, R., de Lera Acedo, E., Zarb Adami, K., Alderighi, M., Belli, C., et al. (2021). The aperture array verification system 1: System overview and early commissioning results. *Astronomy & Astrophysics*, *655*, A5. https://doi.org/10.1051/0004-6361/202040086

Bolli, P., Bercigli, M., Di Ninni, P., Mezzadrelli, L., & Virone, G. (2022). Impact of mutual coupling between SKALA4.1 antennas to the spectral smoothness response. *Journal of Astronomical Telescopes, Instruments, and Systems*, *8*(01), 011023. https://doi.org/10.1117/1.JATIS.8.1.011023

Bolli, P., Mezzadrelli, L., Monari, J., Perini, F., Tibaldi, A., Virone, G., et al. (2020). Test-driven design of an active dual-polarized log-periodic antenna for the square kilometre array. *IEEE Open Journal of Antennas and Propagation*, *1*, 253–263. https://doi.org/10.1109/OJAP.2020.2999109

Caiazzo, M. (2017). *SKA phase 1 system requirements specification (technical report no. SKA-TEL-SKO-0000008)*. SKAO. Retrieved from https://www.skao.int/sites/default/files/documents/d3-SKA-TEL-SKO-0000008-Rev11_SKA1SystemRequirementSpecification.pdf

Comoretto, G., Chiello, R., Roberts, M., Halsall, R., Adami, K. Z., Alderighi, M., et al. (2017). The signal processing firmware for the low frequency aperture array. *Journal of Astronomical Instrumentation*, *6*(1), 1641015. https://doi.org/10.1142/S2251171716410154

Costa, N., & Haykin, S. (2010). Multiple-input, multiple-output channel models. https://doi.org/10.1002/9780470590676

Davidson, D. B., Bolli, P., Bercigli, M., di Ninni, P., Steiner, R., Tingay, S., et al. (2019). Electromagnetic modelling of the ska-low aavs1.5 prototype. In *2019 international conference on electromagnetics in advanced applications (iceaa)* (pp. 1032–1037). https://doi.org/10.1109/ICEAA.2019.8879294

Dewdney, P. E., & Braun, R. (2016). *SKA1-LOW configuration coordinates—COMPLETE SET (technical report no. SKA-TEL-SKO-0000422)*. SKAO. Retrieved from https://www.skao.int/sites/default/files/documents/d18-SKA-TEL-SKO-0000422_02_SKA1_LowConfigurationCoordinates-1.pdf

Hampson, G. A., Bunton, J. D., Gunst, A. W., Baillie, P., & bij de Vaate, J.-G. (2016). Introduction to the SKA low correlator and beamformer system. In H. J. Hall, R. Gilmozzi, & H. K. Marshall (Eds.), *Ground-based and airborne telescopes vi* (Vol. 9906, p. 99062S). https://doi.org/10.1117/12.2231524

Harris, C. R., Millman, K. J., van der Walt, S. J., Gommers, R., Virtanen, P., Cournapeau, D., et al. (2020). Array programming with NumPy. *Nature*, *585*(7825), 357–362. https://doi.org/10.1038/s41586-020-2649-2

Hunter, J. D. (2007). Matplotlib: A 2d graphics environment. *Computing in Science & Engineering*, *9*(3), 90–95. https://doi.org/10.1109/MCSE.2007.55

Kiefner, U., Wayth, R. B., Davidson, D. B., & Sokolowski, M. (2021). Holographic calibration of phased array telescopes. *Radio Science*, *56*(5), e07171. https://doi.org/10.1029/2020RS007171

Kolda, T. G., & Bader, B. W. (2009). Tensor decompositions and applications. *SIAM Review*, *51*(3), 455–500. https://doi.org/10.1137/07070111X

Macario, G., Pupillo, G., Bernardi, G., Bolli, P., Di Ninni, P., Comoretto, G., et al. (2022). Characterization of the SKA1-low prototype station aperture array verification system 2. *Journal of Astronomical Telescopes, Instruments, and Systems*, *8*(01), 011014. https://doi.org/10.1117/1.JATIS.8.1.011014

McKinney, W. (2010). Data structures for statistical computing in Python. In S. van der Walt & J. Millman (Eds.), *Proceedings of the 9th Python in science conference* (pp. 56–61). https://doi.org/10.25080/Majora-92bf1922-00a

Misner, C. W., Thorne, K. S., & Wheeler, J. A. (1973). Gravitation.

Naldi, G., Mattana, A., Pastore, S., Alderighi, M., Zarb Adami, K., Schillirò, F., et al. (2017). The digital signal processing platform for the low frequency aperture array: Preliminary results on the data acquisition unit. *Journal of Astronomical Instrumentation*, *6*(1), 1641014. https://doi.org/10.1142/S2251171716410142

Price-Whelan, A. M., Price-Whelan, A. M., Sipőcz, B. M., Günther, H. M., Lim, P. L., Crawford, S. M., et al. (2018). The astropy project: Building an open-science project and status of the v2.0 core package. *The Astronomical Journal*, *156*(3), 123. https://doi.org/10.3847/1538-3881/aabc4f

Robitaille, T. P., Robitaille, T. P., Tollerud, E. J., Greenfield, P., Droettboom, M., Bray, E., et al. (2013). Astropy: A community Python package for astronomy. *Astronomy & Astrophysics*, *558*, A33. https://doi.org/10.1051/0004-6361/201322068

Salas, P., Brentjens, M. A., Bordenave, D. D., Oonk, J. B. R., & Röttgering, H. J. A. (2020). Tied-array holography with LOFAR. *Astronomy & Astrophysics*, *635*, A207. https://doi.org/10.1051/0004-6361/201935670

Sault, R. J., Teuben, P. J., & Wright, M. C. H. (1995). A retrospective view of MIRIAD. In R. A. Shaw, H. E. Payne, & J. J. E. Hayes (Eds.), *Astronomical data analysis software and systems iv* (Vol. 77, p.433).

Scott, P. F., & Ryle, M. (1977). A rapid method for measuring the figure of a radio telescope reflector. *Monthly Notices of the Royal Astronomical Society*, *178*(4), 539–545. https://doi.org/10.1093/mnras/178.4.539

Sokolowski, M., Wayth, R. B., Bhat, N. D. R., Price, D., Broderick, J. W., Bernardi, G., et al. (2021). A Southern-Hemisphere all-sky radio transient monitor for SKA-Low prototype stations. *Publications of the Astronomical Society of Australia*, *38*, e023. https://doi.org/10.1017/pasa.2021.16

Thekkeppattu, J. N., Wayth, R. B., & Sokolowski, M. (2023). Calibration of an ska-low prototype station using holographic techniques [Dataset]. Zenodo. https://doi.org/10.5281/zenodo.8237885

The Pandas Development Team. (2023). pandas-dev/pandas: Pandas. *Zenodo*. https://doi.org/10.5281/zenodo.3509134

van Es, A. J. J., Labate, M. G., Waterson, M. F., Monari, J., Bolli, P., Davidson, D., et al. (2020). A prototype model for evaluating SKA-LOW station calibration. In H. K. Marshall, J. Spyromilio, & T. Usuda (Eds.), *Ground-based and airborne telescopes viii* (Vol. 11445, p. 1144589). https://doi.org/10.1117/12.2562391

van Haarlem, M. P., Wise, M. W., Gunst, A. W., Heald, G., McKean, J. P., Hessels, J. W. T., et al. (2013). LOFAR: The LOw-Frequency ARray. *Astronomy & Astrophysics*, *556*, A2. https://doi.org/10.1051/0004-6361/201220873

van Straten, W., Jameson, A., & Osłowski, S. (2021). PSRDADA: Distributed acquisition and data analysis for radio astronomy. In *Astrophysics source code library, record ascl:2110.003*.

Waskom, M. L. (2021). Seaborn: Statistical data visualization. *Journal of Open Source Software*, *6*(60), 3021. https://doi.org/10.21105/joss.03021

Wayth, R., Sokolowski, M., Broderick, J., Tingay, S. J., Bhushan, R., Booler, T., et al. (2022). Engineering development array 2: Design, performance, and lessons from an SKA-low prototype station. *Journal of Astronomical Telescopes, Instruments, and Systems*, *8*(01), 011010. https://doi.org/10.1117/1.JATIS.8.1.011010

Wijnholds, S. J. (2017). Calibration of mid-frequency aperture array stations using self-holography. In *2017 international conference on electromagnetics in advanced applications (ICEAA)* (pp. 967–970). https://doi.org/10.1109/ICEAA.2017.8065418

Wijnholds, S. J. (2021). Generalised self-holography. In *2021 xxxivth general assembly and scientific symposium of the international union of radio science (URSI GASS)* (pp. 1–4). https://doi.org/10.23919/URSIGASS51995.2021.9560415

Wilke, C. R., Wijnholds, S. J., & Gilmore, J. (2021). Calibratability of aperture arrays using self-holography. *IEEE Transactions on Antennas and Propagation*, *69*(8), 4527–4537. https://doi.org/10.1109/TAP.2021.3060070

Wilke, C. R., Wijnholds, S. J., & Gilmore, J. (2022). Calibratability of mid-frequency aperture arrays with self-holography. *Journal of Astronomical Telescopes, Instruments, and Systems*, *8*(01), 011008. https://doi.org/10.1117/1.JATIS.8.1.011008